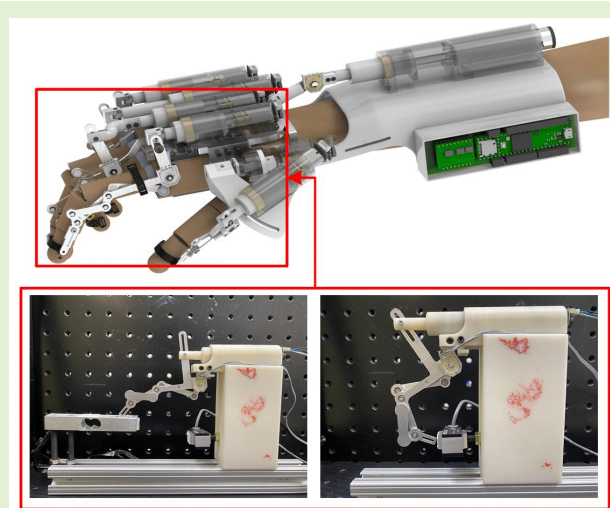


Data Driven Calibration and Control of Compact Lightweight Series Elastic Actuators for Robotic Exoskeleton Gloves

Yunfei Guo¹, Wenda Xu, Sarthark Pradhan, Cesar Bravo, and Pinhas Ben-Tzvi², *Senior Member, IEEE*

Abstract—The working principle of a SEA is based on using an elastic material connected serially to the mechanical power source to simulate the dynamic behavior of a human muscle. Due to weight and size limitations of a wearable robotic exoskeleton, the hardware design of the SEA is limited. Compact and lightweight SEAs usually have noisy signal output, and can easily be deformed. This paper uses a compact lightweight SEA designed for exoskeleton gloves to demonstrate immeasurable strain and friction force which can cause an average of 34.31% and maximum of 44.7% difference in force measurement on such SEAs. This paper proposes two data driven machine learning methods to accurately calibrate and control SEAs. The multi-layer perception (MLP) method can reduce the average force measurement error to 10.18% and maximum error to 29.13%. The surface fitting method (SF) method can reduce the average force measurement error to 8.06% and maximum error to 35.72%. In control experiments, the weighted MLP method achieves an average of 0.21N force control difference, and the SF method achieves an average of 0.29N force control difference on the finger tips of the exoskeleton glove.

Index Terms—Tactile sensor, SEA calibration, exoskeleton glove.



I. INTRODUCTION

A. Exoskeleton and Tactile Sensors

CLOSE to 19.9 million people in the U.S. suffer from hand-related disabilities and have difficulty grasping objects for day-to-day activities [1]. Building an affordable robotic exoskeleton glove that can help these individuals

Manuscript received June 26, 2021; accepted July 13, 2021. Date of publication July 30, 2021; date of current version October 1, 2021. Research reported in this publication was supported by the Eunice Kennedy Shriver National Institute of Child Health & Human Development of the National Institutes of Health under Award Number R21HD095027. The content is solely the responsibility of the authors and does not necessarily represent the official views of the National Institutes of Health. The associate editor coordinating the review of this article and approving it for publication was Prof. Subhas C. Mukhopadhyay. (Corresponding author: Pinhas Ben-Tzvi.)

Yunfei Guo is with the Electrical and Computer Engineering Department, Virginia Tech, Blacksburg, VA 24060 USA (e-mail: yunfei96@vt.edu).

Wenda Xu and Sarthark Pradhan are with the Mechanical Engineering Department, Virginia Tech, Blacksburg, VA 24060 USA (e-mail: wenda@vt.edu; sp21@vt.edu).

Cesar Bravo is with the Carilion Clinic Institute of Orthopaedics and Neurosciences, Virginia Tech Carilion School of Medicine, Roanoke, VA 24016 USA (e-mail: cjbravo@carilionclinic.org).

Pinhas Ben-Tzvi is with the Mechanical Engineering Department and Electrical Engineering Department, Virginia Tech, Blacksburg, VA 24060 USA (e-mail: bentzvi@vt.edu).

Digital Object Identifier 10.1109/JSEN.2021.3101143

perform grasping-related tasks regularly encountered in their daily lives could significantly improve their quality of life.

Lee designed and integrated the iSAFER glove using rigid linkage and cable transmission with two force-sensitive resistors (FSR) on both the fingernail and finger pad side to adapt to the contact angle change [2]. However, FSRs suffer from issues related to repeatability [3]. There are over $\pm 50\%$ errors on random raw data of FSR force sensors.

Ma, *et al.* designed a robotic exoskeleton glove using rigid actuators and side-mounted strain gauges as a tactile sensor to perform force control [4]. The advantages of using strain gauges include comfort and their compact size. However, this method requires calibration for each user to achieve an accurate result.

Diez, *et al.* proposed a novel design of a robotic exoskeleton using an optical force sensor as a tactile sensor, which resolved the accuracy problem when using FSRs [5]. This approach could be a great solution, except that the sensor's size is too large for an exoskeleton glove application.

B. Series Elastic Actuators

Using Series Elastic Actuators (SEA) may be a practical option for a high accuracy exoskeleton glove after reviewing the previous methods. The original SEA design was proposed

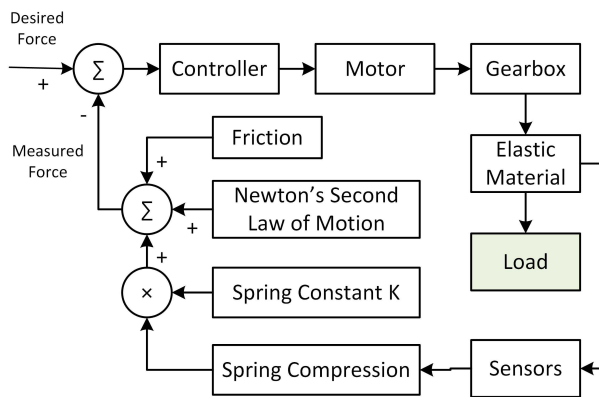


Fig. 1. Series elastic actuator working principle flowchart.

by the MIT Artificial Intelligence Laboratory in 1995 [6]. In the original design, a torsion spring is connected in series between the output shaft of an electric motor and the SEA output shaft. The output force is calculated by measuring the angle of twist in the torsion spring. Compared to rigid actuators, advantages of using SEAs include accurate force sensing and wider control bandwidth. Springs provide more linear and repeatable force-sensing than FSRs. Springs can also act as low-pass filters to filter out the high-frequency motion, reducing the control speed leading to wider control bandwidth. The structure and force calculation of SEAs is explained in Fig.1. Following the original SEA design, a wide variety of SEAs have been used in robotic exoskeletons. Kim, *et al.* designed hydraulic SEAs to be used in exoskeleton assisted walking, and sit-to-stand (SIT) motions [7]. Karavas, *et al.* designed electric SEAs for joints used in lower limb exoskeletons [8]. Those designs provide accurate force control and high output force. However, those designs required large hydraulic or electric power sources with metal housings and output shafts. The main challenges of applying the SEAs mentioned above to a robotic exoskeleton glove are the size and weight.

Work done in previous research built several lightweight, compact SEAs for robotic exoskeleton gloves to reduce the size and weight. The primary purpose of using SEAs on an exoskeleton glove is as tactile sensors to provide accurate force measuring. Proper force measuring on fingertips using SEAs requires high rigidity of the elastic material's exoskeleton and low stiffness. High rigidity usually leads to bulky designs, and low stiffness will restrict the maximum output force. Most of the previous research either suffered from inaccurate force feedback due to the deformation of the exoskeleton or deficient force output that cannot fulfill user needs.

Force calibration is essential for performing force feedback control with SEAs. The feedback control will not work without calculating the correct amount of force generated by the SEA.

This paper proposes a method to calibrate and design a control scheme for compact, lightweight SEAs using multi-layer perception (MLP). Implementing the MLP method is then compared against those found using a surface fitting (SF) approach, which is considered a commonly used technique. After calibration, these SEAs can be used as accurate tactile sensors on a robotic exoskeleton glove. The calibration meth-

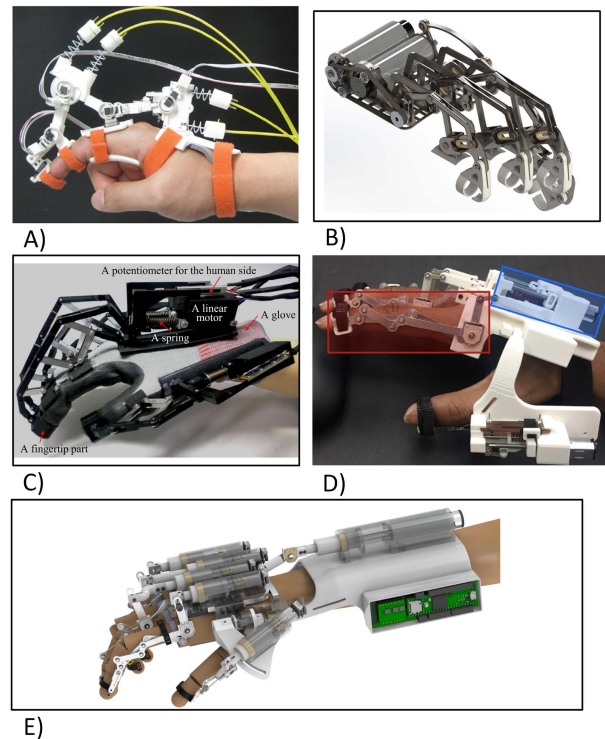


Fig. 2. Five existing examples of SEA and Exoskeleton Glove: A) An index finger exoskeleton with series elastic actuation for rehabilitation [9]. B) Series Elastic Transmission hand exoskeletons [10]. C) A wearable and force-controllable hand exoskeleton system [11]. D) A general purpose robotic hand exoskeleton with series elastic actuation [12]. E) A robotic glove system for patients with brachial plexus injuries [13].

ods proposed in this paper can be easily applied to SEAs with similar structures.

II. LITERATURE REVIEW

Researchers have been working for years to develop SEAs for exoskeleton gloves.

Bianchi, *et al.* proposed a novel design of a titanium alloy exoskeleton glove with SEA using elastic material with very high stiffness [10]. This design is shown in sub-figure (B) of Fig.2. The exoskeleton can output 20N of force on each fingertip. There are three main disadvantages with this design. First, due to the high force output of the SEA, the size of the motor used on such SEA needs to be powerful, but large in size. The size of the exoskeleton limited the number of motors that can be used. The design coupled the middle, ring, and little finger into one motion to keep the design compact. However, those design features reduced the degrees of freedom (DOFs) of such gloves. Second, the use of a high stiffness elastic material makes the goal of accurate force measurement much more challenging to achieve. Instead of using a normal spring-like SEA, this design used a very high stiffness elastic material. The elastic material has a stiffness constant of 58 N/mm. This paper does not propose a valid control structure for high stiffness force feedback control. Third, the titanium alloy needed to meet the rigidity requirements brought on by using a high stiffness elastic material significantly increases the cost to manufacture such an exoskeleton.

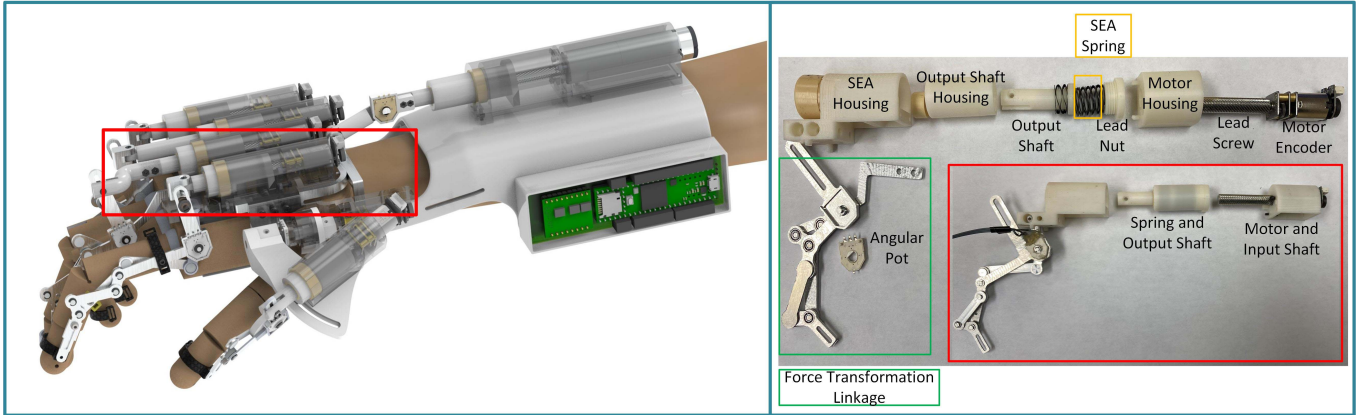


Fig. 3. The construction of the SEA and exoskeleton used in this research.

Agarwal, *et al.* designed a cable-driven exoskeleton with rigid linkage using two SEAs on each finger [9]. This previous design is shown in sub-figure A of Fig.2. Force control used in this previous research has about 10% error and can output 0.3Nm peak torque on each SEA output joint. The main issues with this design are the size and weight. To output 0.3Nm torque to one finger requires the use of two large RE-Max 29 motors. The user needs to carry the power source (motor, motor pulley, battery), which dramatically reduces mobility.

Jo, *et al.* designed a compact linear SEA for use in robotic exoskeleton gloves [11]. This design is shown in sub-figure C of Fig.2. Accurate force control is achieved with a linear-quadratic (LQ) tuned proportional-derivative (PD) controller to control the distance and a disturbance observer (DOB) to model the uncertainty. However, the spring constant is very low (0.343 N/mm), which results in a maximum output force of 9N to the SEA output shaft. In contrast, a normal healthy 20-29-year-old male can output a maximum of 450N on all fingers, which is about 90N on each fingertip [14].

Refour *et al.* designed a compact linear SEA for robotic exoskeleton gloves, which can output 20N on each fingertip [12]. This design is shown in sub-figure D of Fig.2. One of the main issues with this design is force accuracy. According to the author, the SEA experiences 2-3N of output force error. This error is measured at the SEA output shaft, which does not include the error caused by the linkage mechanism itself. Due to the unaccounted deformation of the plastic SEA housing and thin aluminum linkage, the force output on the fingertips may be inaccurate. Because of the inaccuracy in force output on the fingertips, it may not be effective to sacrifice the SEA's space over FSRs.

Xu, *et al.* proposed a low-cost, compact, lightweight SEA used in the RML exoskeleton [13]. This design is shown in sub-figure E of Fig.2. This SEA has a high force output of 40N at the SEA output shaft and 20N at each fingertip. This size is desirable for exoskeleton applications. However, this SEA suffered from rigidity and accuracy problems which affected many of the other designs discussed previously. It uses thin aluminum linkages with 3D printed plastic motor output shafts and housing. Due to the high output and low rigidity,

the linkage motor output shaft on the SEA will deform. This deformation causes the force output of the SEA to be non-linear in relation to the strain of the elastic material in the SEA.

III. SEA FORCE MODELING

This paper uses the SEA design presented in Xu, *et al.*'s paper [13] as an example. This SEA is compact, lightweight, low-cost, and provides sufficient force output (Maximum 20N on fingertips). However, it exhibits noisy sensor reading, hard-to-measure friction force, a back drive-able motor, and deformable linkages and SEA housing. These characteristics make this SEA a good candidate to demonstrate the difficulty of using traditional kinematics model-based calibration. The SEA and exoskeleton overview is shown in 3. The index finger SEA is used as an example to demonstrate the force calculation.

A. Series Elastic (SEA) Actuator Construction

The compact, lightweight SEA built for the RML glove consists of a linear actuator and a linkage. Force on the fingertips can be measured when these two parts are combined. The first part is a regular elastic linear actuator with motor, gearbox, lead screw, lead nut, spring, and output shaft. The second part is an aluminum linkage that transfer force from the linear actuator's output shaft to the fingertips. Both parts are described in the linear SEA portion of Fig.3.

B. SEA Force Calculation

The index finger SEA is showed in Fig.4. Theoretically, when the SEA is not moving, the force can be calculated by Eq.1. The encoder can sense the distance between DE and the potentiometer can sense $\angle ABC$. CB and CE are constant and can be directly measured. δl_s can be calculated by Eq.2. F_{fa} and F_{fl} can be compensated for with a constant value during force calibration. R_l is a variable that changes as the linkage angle changes. The ratio varies for different force measuring methods. This ratio is discussed in the following section.

$$F_t = (\delta l_s \times k_s - F_{fa}) \times R_l - F_{fl} \quad (1)$$

$$\delta l_s = \cos(\angle ABC) \times CB - (DE - CE) \quad (2)$$

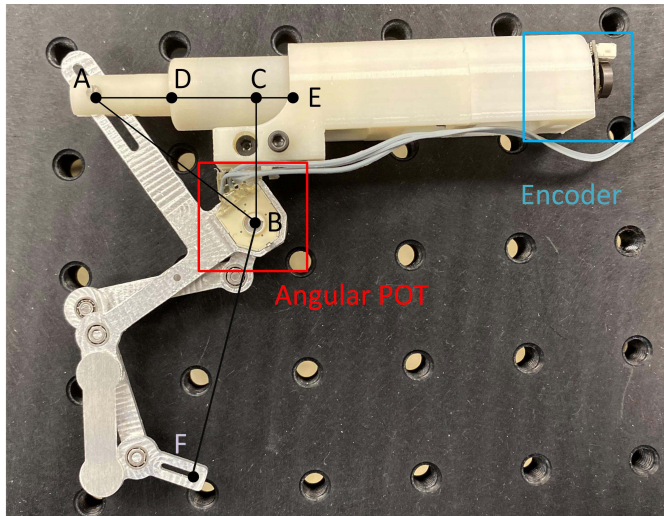


Fig. 4. SEA force calculation legend.

F_t – force on linkage tip, perpendicular to the last linkage
 δl_s – spring compression
 F_{fa} – friction force of actuator
 R_l – SEA to linkage force transformation ratio
 F_{fl} – friction force of linkage

C. Encoder

A 12 CPR Pololu quadrature magnetic encoder is attached to a 12v Pololu micro-gear motor paired with a 380:1 gearbox. The lead screw has a distance (mm) to revolution ratio of 20:1. The actuator shaft movement δDE in millimeters can be calculated by Eq.3.

$$\delta DE = \frac{R_{ld}}{N_{cpr}} \times N_{enc} = \frac{20}{380} \times N_{enc} \approx 0.00438596 \times N_{enc} \quad (3)$$

δDE – displacement of DE measured in millimeters
 R_{ld} – distance to revolution ratio of lead screw, 20mm:1rev
 R_g – output shaft to input shaft ratio of gearbox, 380:1
 N_{cpr} – count per revolution of encoder, 12
 N_{enc} – encoder count

D. Angular Potentiometer

A 15 to 345-degree angular potentiometer is placed on the linkage to measure the linkage angle. Such potentiometer is read through a 3.3v 12 bit ADC bus. This potentiometer's voltage is increased to 20.5v for better resolution. Due to the voltage, the effective range can be calculated using Eq.4. A 20 degrees mechanical offset is introduced to avoid over-voltage damage to the micro-controller. $\angle ABC$ is calculated by Eq.5.

$$ER_{pot} = \frac{V_{adc}}{V_s} \times R_{pot} = \frac{3.3}{20.5} \times 330^\circ \approx 53.12195^\circ \quad (4)$$

$$\angle ABC = \frac{ER_{pot}}{Re_{adc}} \times Pot - \angle O + \angle S$$

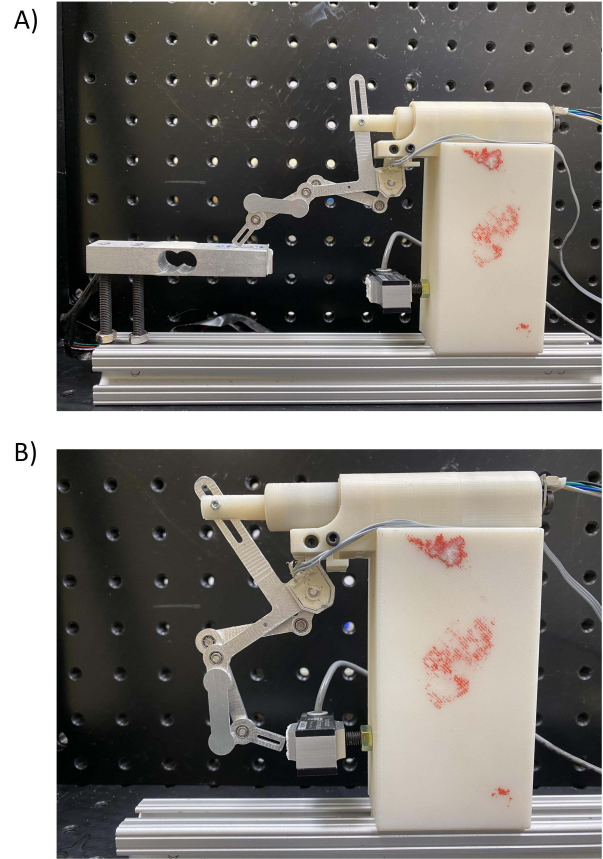


Fig. 5. A) Horizontal mounted load cell used for force measurement, B) Vertical mounted load cell used for force measurement.

$$\approx \frac{53.12195^\circ}{2^{12}} \times Pot - 20^\circ + 15^\circ \approx 0.012969 \times Pot - 5^\circ \quad (5)$$

ER_{pot} – effective measuring range of potentiometer
 V_{adc} – adc bus reference voltage, 3.3v
 V_s – source voltage of potentiometer, 20.5v
 R_{pot} – measuring range of potentiometer, 330 degrees
 Re_{adc} – adc resolution, 12bit, 4096
 Pot – raw potentiometer adc reading
 $\angle O$ – potentiometer offset angle, 20 degrees
 $\angle S$ – potentiometer start angle, 15 degrees

E. Force Measurement

Force measurement is usually performed using a load cell. However, measuring force directly from the linkage end can be complicated as it is difficult to place the load cell perpendicular to the last linkage. In this research, the force is measured by two different load cells placed at a different location to accommodate the linkage at different angles. The mounting position is shown in Fig. 5. The force measured at the linkage end is transformed back to the actuator output shaft through inverse kinematics.

F. Linkage Force Transformation Ratio

The linkage design is based on [15]'s optimization. The linkages force transformation ratio (R_l) is critical for calculating the fingertips' force. When the last linkage's contact angle

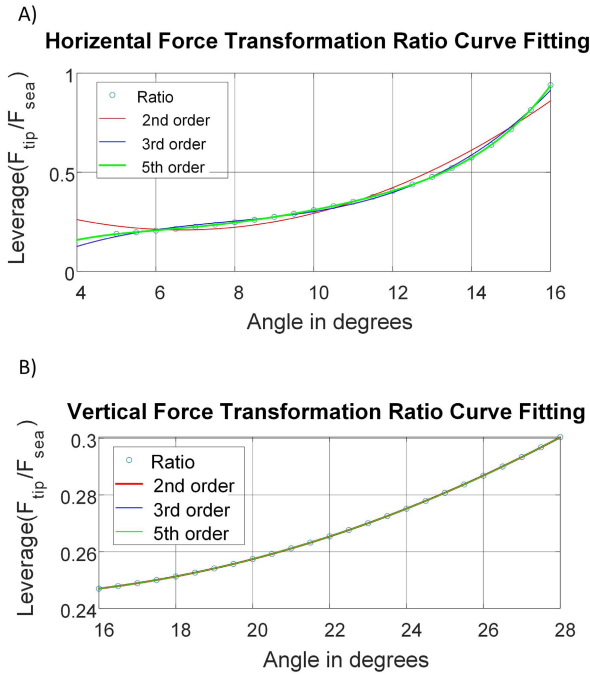


Fig. 6. A) Small angle linkage transformation B) Large angle linkage transformation.

is less than 90 degrees, the load cell is mounted horizontally. When the last linkage's contact angle is more than 90 degrees, the load cell is mounted vertically. The relationship between angle and the linkage force transformation ratio (R_l) is shown in Fig.6. The horizontal linkage force transformation ratio is described as a fifth-order equation (H_{fit}), and the vertical linkage force transformation ratio is described as a second-order equation (V_{fit}). The combined equation is shown in Eq.6.

$$R_l = \begin{cases} H_{fit} & \text{if } 5^\circ \leq \angle ABC \leq 16^\circ \\ V_{fit} & \text{if } 16^\circ < \angle ABC \leq 28^\circ \end{cases} \quad (6)$$

IV. CHALLENGES WITH SEA FORCE CALIBRATION

Based on the previous section, the force output of the SEA should be easy to calculate. PID position control is used to drive the SEA. The calculated force is compared with the measured force from a load cell.

Theoretically, the measured force and calculated force should be similar. However, when testing the SEA, the measured force and calculated force have up to around 45% difference in value. There exist two major problems that the previous research has not addressed: friction and deformation, which are discussed in the following subsections.

A. Friction Force on the Actuator

The spring constant of the spring used in this SEA is 4.2 N/mm. Using the traditional SEA force calculation that the previous researchers used, the output force should match the calculated force without the linkage affecting it. However, the experimental result in Fig. 7 showed that the measured force was generally lower than the calculated force because

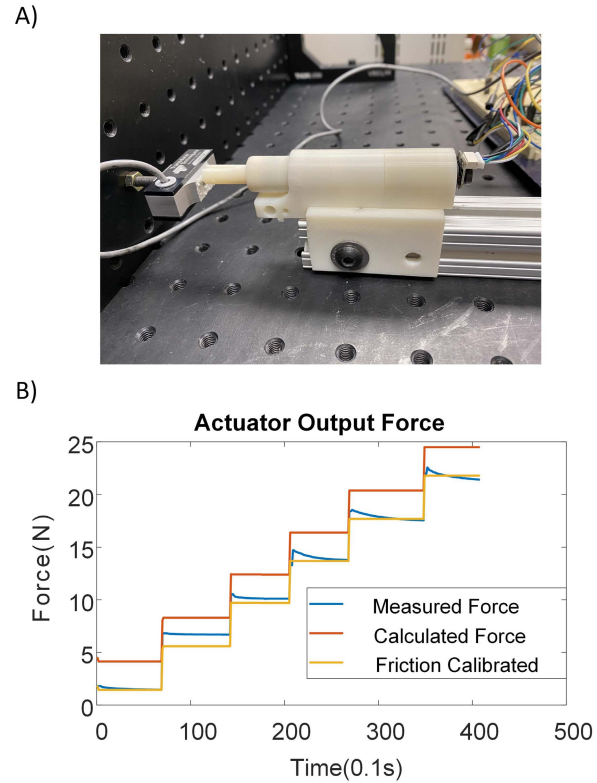


Fig. 7. Difference of the output force and measured force due to friction. Measured friction force is 2.7N (0.68mm spring compression).

there exists a large amount of frictional force that affects the output force.

B. Combined Friction Force of the Linkage and the Actuator

The friction force has a significant impact on the output force. This experiment is to find the combined friction force caused by the linkage and the actuator. During this experiment, the SEA with the linkage is actuated against a load cell at various angles. The measured compression from the SEA will increase, but the load cell's reading remains zero. The load cell's reading will not be zero when the applied force is greater than friction force, and the measured compression represents the amount of friction force. Fig. 8 shows that the friction force varies at different angles.

C. Actuator Shaft and Linkage Deformation

Theoretically, if the friction force is calibrated at a different angle, the commanded output force should match the measured force. However, the measured force was still significantly smaller than the commanded force.

The difference is due to two parts on the SEA deforming when force is applied. The resulting strain reduces the force output to the fingertips. In Fig.9 part A, the actuator output force is measured without the linkage attached. The encoder reading remains the same, but the force starts to decrease. In part B, the calculated force is calibrated for the measured friction force. However, there exists over 48% difference

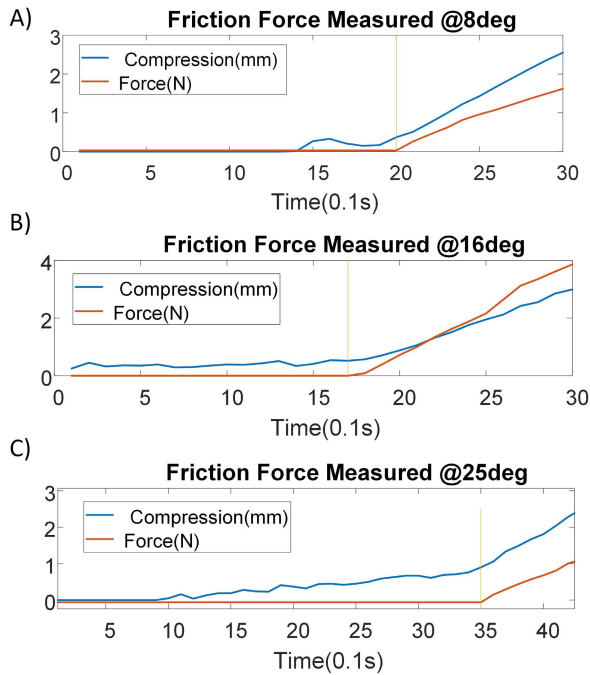


Fig. 8. Different friction force measurement at different angles. **A)** Friction is 2.1N (0.51mm spring compression), **B)** Friction is 2.4N (0.57mm spring compression), **C)** Friction is 4.45N (1.06mm spring compression).

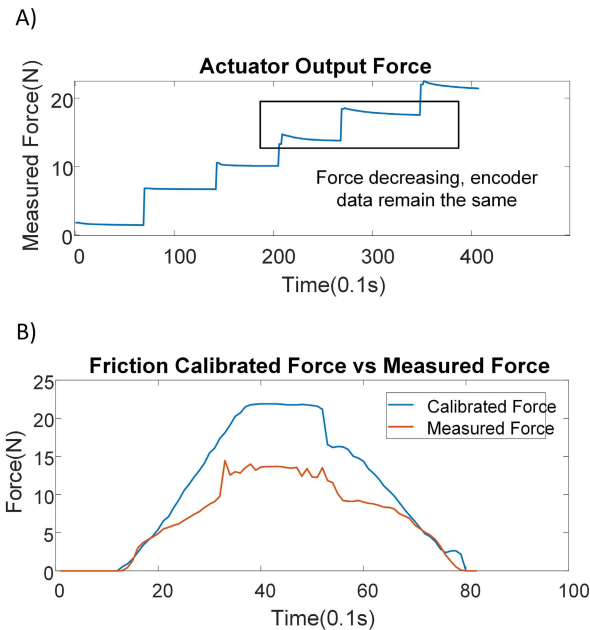


Fig. 9. Force measurement error caused by deformation **A)** Inconsistency in force measurement caused by actuator shaft deformation, **B)** Force measurement error caused by linkage deformation.

between the measured and computed force. This experiment also showed that the difference increases as the force increases.

V. FORCE CALIBRATION

Upper part in Fig.10 shows the kinematics calculation of traditional force feedback control. According to experiments in the previous section, sensor readings, spring compression, and linkage transformation ratios are marked as yellow, which means that these parts will have a small error due to sensor

noise. Newton’s Second Law of Motion is marked in blue, indicating that it can be ignored due to the small mass of the moving parts. The friction force and forces caused by the deformation from the linkage and actuator output shaft are difficult to measure. Thus, these are marked as immeasurable. When combined, the error from sensors and immeasurable values create a large error in the feedback force.

To solve this problem, the linkage and actuator need to be viewed as a whole system and calibrated using a data driven machine learning method based on load cell measurements.

A. Multi-Layer Perception Approach Force Predictor

A multi-layer perception model is used to predict the output force based on the sensor reading. The network is shown in 10. Except for the friction force and deformation of the actuator shaft and linkage, the model will also take acceleration and speed into consideration. The friction force has a different direction while moving, and might be different under different speeds and accelerations. Thus, the network has nine inputs, including the raw potentiometer reading, the raw encoder reading, the calculated spring compression, and the above variables’ speeds and accelerations.

B. Network Tuning and Lost Function Selection

The calibration network is adjusted using hyper-parameter tuning. The hyper-parameter tuning is focused on finding the best layer, number of nodes, and cost function combination. Two standard cost functions are compared.

The mean absolute error (MAE) is shown in Eq. 7. The error measures the absolute difference between the prediction and measured value. In this case, the difference means the difference in force.

$$E = \frac{1}{n} \sum_{j=1}^n |y_j - \hat{y}_j| \tag{7}$$

The mean squared error (MSE) is shown in Eq. 8. The error measures the square of the difference between the prediction and measured value. This method punished outlier data more than the MAE error.

$$E = \frac{1}{n} \sum_{j=1}^n (y_j - \hat{y}_j)^2 \tag{8}$$

VI. FORCE CONTROL

When controlling the SEA, traditional force feedback control will not work well due to the low control frequency. In a compact design mentioned in Xu, *et al.*’s [13] paper, the onboard micro-controllers run ten threads and control seven different SEAs, which means it does not have the computational power to run the prediction network. Cloud computing is required for prediction networks, but the delay in cloud computing restricts the control speed. The control frequency is set to 10Hz due to the limitation of wireless connection over Bluetooth. The control is divided into two parts: A high-level spring compression predictor based on force sensor readings and a low-level compression controller.

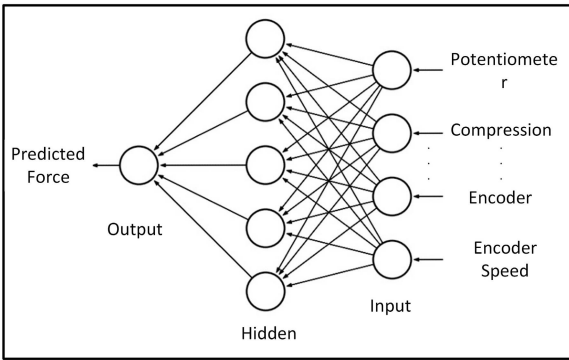
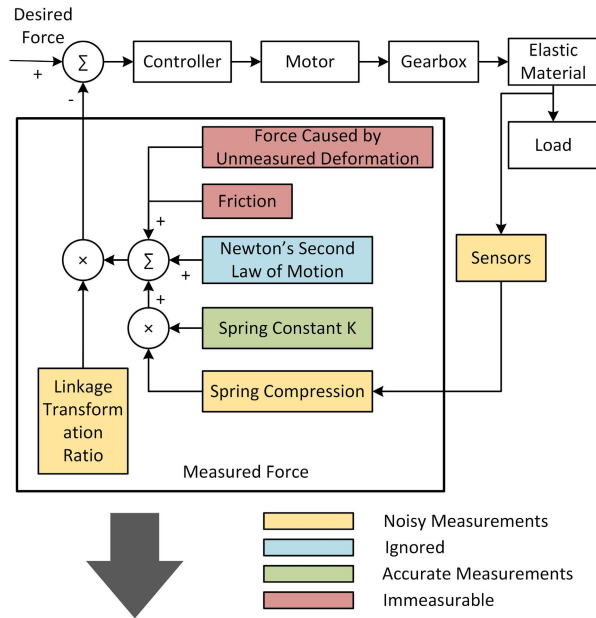


Fig. 10. Inaccurate kinematics calculation can be replaced by data driven machine learning method to improve accuracy.

A. Low-Level Control Method and Control Margin

The low-level PID spring compression control runs on the micro-controller. This low-level controller can ensure accurate control of the spring compression and SEA position. This low-level controller is also used as a safety feature to ensure that the motor works correctly even when the wireless connection is cut off.

The SEA used in this research has a noisy sensor reading due to an analog sensor. The reference voltage fluctuates a little bit, causing a loud sensor reading. Using a noisy angular potentiometer directly as the low-level control input will cause the compression reading to oscillate as the potentiometer reading fluctuates.

The DC motor used in this research has a maximum speed of 32,300 RPM with a low-resolution 12-bit CPR encoder attached to the motor shaft. Twenty encoder counts are equivalent to 0.1 mm in linear actuation. A 0.1 mm difference is equivalent to around 0.5N output force from the actuator output shaft. The requirement of accuracy in motor control is very high.

The position control of the motor is separated from the potentiometer reading to solve the fluctuating sensor reading. The control structure is described in Fig.12. The PID motor

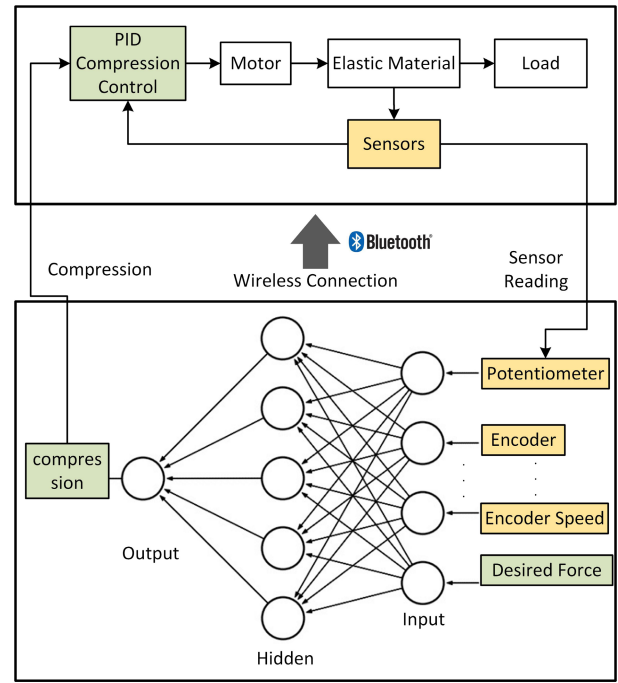


Fig. 11. Flowchart demonstrates feed forward SEA finger tip force control using multi-layer perception compression prediction.

position control runs at 100Hz to ensure accuracy, while the averaged potentiometer reading is updated at 10Hz. The control margin is set to 0.1mm compression difference to avoid oscillation.

B. High Level Multi-Layer Perception Compression Predictor

This compression predictor is modified based on the force calibration network. The network has seven inputs, including the raw potentiometer reading, the raw encoder reading, compression, the speeds and accelerations of the above variables, and the desired force. The network is trained using the same data used for calibration and is tuned using a hyperparameter tuning method. This network can predict the desired compression based on the current data. However, due to the different linkage angles and friction force, the predicted data is not accurate. New data is fed into the predictor to update the predicted compression. The desired compression is sent to the low-level compression controller to perform accurate compression control.

C. Weighted Input Compression Predictor

In the real world, these input data fields do not weigh equally. The desired force has a more significant impact on the compression, and the angle and SEA travel distance have less impact. The acceleration and speed have a low effect on the compression. The input can be weighted to increase the accuracy and robustness of the model. The weight of each factor can be taken as a tuning parameter.

VII. SURFACE FITTING

To compare the performance of the multi-layer perception (MLP) approach, a commonly used, low computational

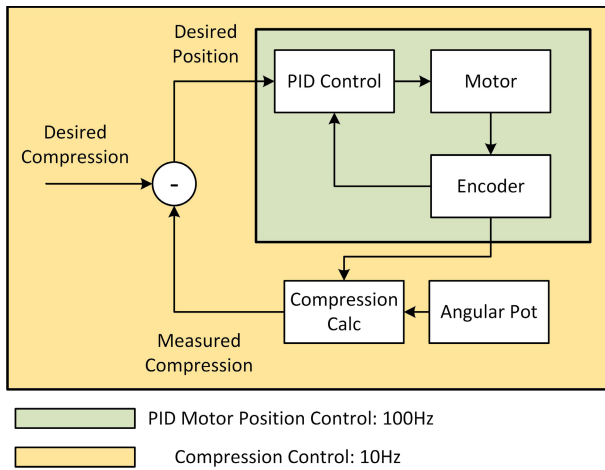


Fig. 12. Micro-controller level compression control structure flowchart.

cost surface fitting approach is used as a comparison method for calibration and control.

A. Calibration

For calibration, the inputs are angle and compression, and the result will be the output force. The advantage of this approach is the low computational cost. This method is suitable for calibrating multiple SEAs in parallel on one micro-controller. The disadvantage is that the speed and acceleration are not taken into consideration which might affect accuracy. When moving in different directions, the friction force also acts in different directions. This method does not consider friction force direction. This method does not use as much computational power as the MLP approach by having fewer inputs and only third-order linear regression. As a trade-off, the accuracy might be lower.

B. Control

For controlling the SEA, this method can be used as a direct substitute for the high-level multi-layer perception approach, while the low-level control remains the same. Instead of running on a separate computer and sending results back to the micro-controller through a wireless connection, this method can run on the micro-controller itself.

VIII. EXPERIMENTS AND RESULTS

A. Data Preparation

The data is collected using a load cell. As described in the previous force measurement section, two load cells measure force in different directions, and as such there are two different reference force values based on two different directions. The measured data must be pre-processed to be suitable for training. We transform the force at the fingertip back to the SEA output shaft using the linkage transformation ratio. The force at the SEA output shaft is used as the reference value. This value includes the deformation of the linkage, SEA output shaft, and friction force. Using this model, we can assume that the system is ideal where no friction and deformation need to be considered.

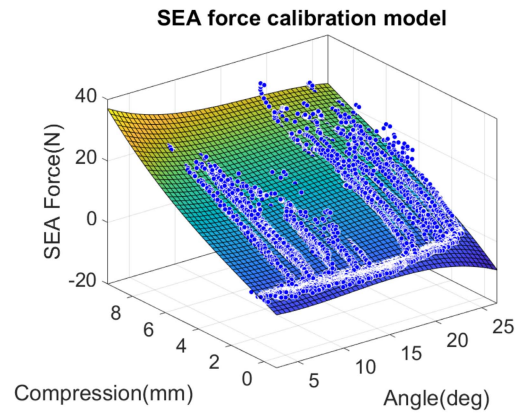


Fig. 13. Surface fitted model (MAE) used for finger tip force calibration.

TABLE I

SEA FINGER TIP FORCE CALIBRATION RESULTS

Method	Loss function	Opt Network Struc	Error
MLP	MSE	16-32	1.432
MLP	MAE	8-16-32	2.13
SF	MSE	N/A	1.855
SF	MAE	N/A	0.987

For example, the force output of a SEA is 10N, while 5N of that is lost in transmission. Thus, the net output force is 5N. After calibration, the result will show that the output is 5N, and it can be assumed that there is no loss in force transmission to the fingertip.

The data set used for training contains 10,400 data points, and the test data has 2,416 data points collected using two load cells. Both the test and training data-set include data collected from 12 different contact angles. We have also collected validation data-set at a randomly selected angle with 140 data points to verify the performance.

B. Force Calibration Results

The surface fitting (SF) model is shown in Fig.13. The fitting used a 3rd order polynomial, and most points are fitted to the surface. This graph shows that the force output is not entirely repeatable. There exists a small amount of error in the force output, even with similar angles and compression.

For multi-layer perception approach (MLP), the hyper-parameter tuning result of each loss function is shown in Tab. I. For the mean absolute error (MAE) loss function, the optimal network has three layers, and each layer has 8,16,32 nodes. For the mean square error (MSE) loss function, the optimal network has two layers, and each layer has 16,32 nodes.

The result of the multi-layer perception (MLP) model is compared with the surface fitting (SF) method over the testing data-set. The results are shown in Tab. I. For the MLP method, using MSE loss function has 22% performance gain over the SF method. When using MAE loss function, the SF is 72.5% more accurate. The MSE loss function of MLP and MAE of SF is selected to do further comparison.

Fig.14 shows a demo of the force prediction using the above two methods over validation data-set. The MLP method using MSE loss function has a better fit under 15N, while the surface fitting has a better fit over 15N.

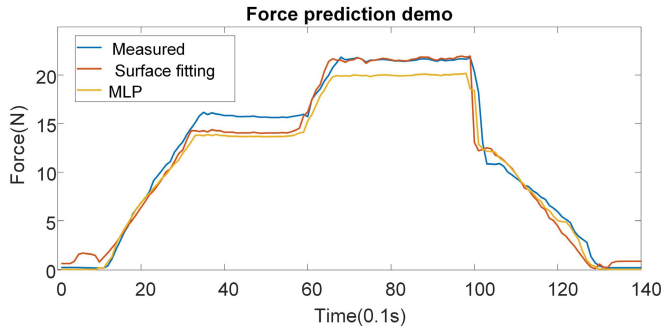


Fig. 14. Force calibration demo on validation data-set.

TABLE II

AVERAGE FORCE CONTROL ERROR AND AVERAGE SETTLING TIME

Force	Method	Force error avg	Settling time avg
5N	SF	0.29N	0.32s
10N	SF	0.41N	0.50s
15N	SF	0.18N	0.58s
5N	MLP	0.24N	2.72s
10N	MLP	0.30N	3.22s
15N	MLP	0.1N	3.15s

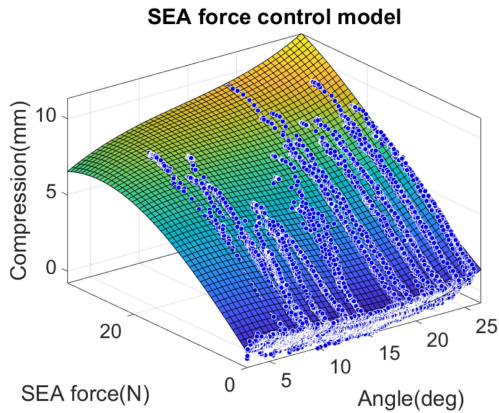


Fig. 15. Surface fitted SEA finger tip force control model (MAE) used for force control.

TABLE III

SEA FINGER TIP FORCE CONTROL RESULTS

Method	Loss function	Opt Network Struc	Error
MLP	MAE	8-16	0.19
MLP	MSE	8-16	0.17
SF	MSE	N/A	0.35
SF	MAE	N/A	0.24

C. Force Control Results

The surface fitting model is shown in Fig. 15. The fitting used 3rd order polynomial, and most points are fitted on the surface. This model describes the relationship between compression, force, and angle.

The weighted MLP approach result is shown in Tab. III. For the MAE loss function, the optimal network consists of two layers, and each layer has 8,16 nodes. For the MSE loss function, the optimal network consists of two layers, and each layer has 8,16 nodes.

The weighted multi-layer perception model result is compared with the surface fitting method's result over the testing data-set. The results are shown in Tab. III. For the weighted MLP method, using both MAE and MSE loss function gives better accuracy than the SF method. Weighted MLP method

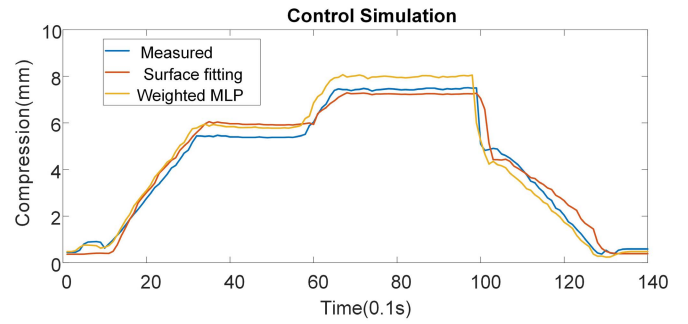


Fig. 16. Force control simulation using validation data-set.

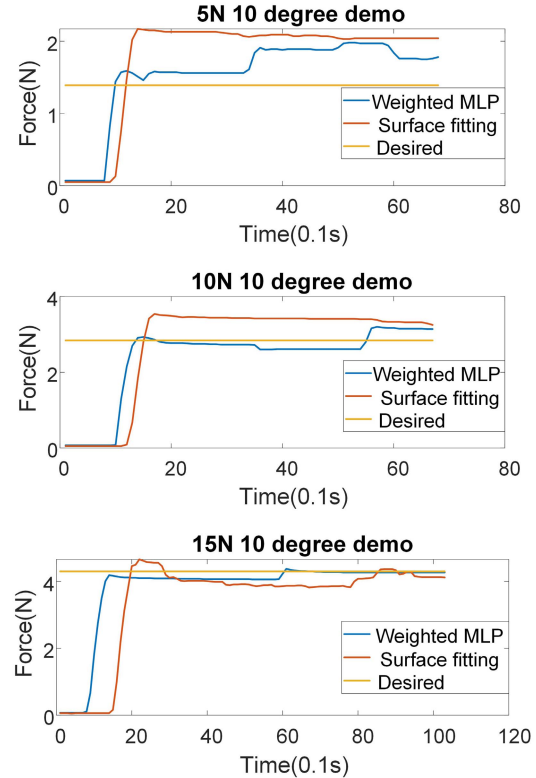


Fig. 17. Force control result using real SEA.

using MSE loss function has 51.4% performance gain over the surface fitting method using MSE loss function. The MLP method using the MAE loss function has a 20.9% performance gain over the SF method using MAE loss function. Thus, we select MSE as the optimal loss function due to higher performance gain over SF method. MAE loss function is selected for SF method due to less performance difference compare to weighted MLP method.

Fig. 16 shows a simulation of force control using the validation data-set with the above two methods. This simulation used measured force to predict the desired compression and compared the predicted compression with the measured compression. The MLP method has a better fit for low compression, while the SF method fits better under higher compression.

Fig. 17 shows the weighted MLP prediction control performance vs. the surface fitting control in the real world. The tests are performed at 10 degrees. The output force on the SEA output shaft is set to 5N, 10N, and 15N. The

desired force on the fingertip is calculated through the linkage transformation ratio. The actual applied force is measured using a load cell. The result shows that the MLP approach has a slightly more accurate force output. The MLP approach has an error within 0.3N, while the SF method has an error within 0.6N. These experiments show that the force control worked as expected when applied to real hardware.

The settling time increases as the output force increases due to longer actuation time. Each control method is used to output 5/10/15N force at ten different contact angles. The linkage starting angle will be at 5 degrees. The settling time is measured when the linkage comes in contact with the load cell and ends when the output reaches 0.3N and 0.6N error bound. The settling time and force error for different angles is averaged and shown in Tab.II.

The force control curve is not so smooth as expected due to the angle measured by the potentiometer being slightly larger than the actual value due to the moving motor's voltage drop. It takes time to drop back to a stable reading and this causes a fluctuation in the reading.

IX. CONCLUSION

This paper proposed two methods to control and calibrate a compact, lightweight linear SEA used in an exoskeleton.

This paper showed that friction force and linkage deformation can cause an average of 34.31%, and a maximum of 44.7% difference in force measurement on the compact, lightweight SEA used in the RML glove. These findings can be applied to most exoskeleton gloves that require force transformation from the SEA to the fingertips. Calibration is necessary for any compact, lightweight SEA used in an exoskeleton glove. This paper proposed two methods for calibration and control of the compact, lightweight SEA.

In calibration test, when using MSE loss function and the test data-set, the MLP method is 22% more accurate. When using MAE loss function, the SF is 72.5% more accurate. When the test is conducted using the validation data-set, both methods show similar performance. MLP method has a slightly higher average difference but smaller maximum difference. Both methods are over 65% more accurate than kinematics calculation calibration. The performance comparison of both method on validation data-set is showed in Tab. IV.

In force control test, the MLP method is more accurate using both MAE and MSE loss function. When using MSE loss function, MLP method is 51.4% more accurate. When using MAE loss function, MLP method is 29.1% more accurate. When tested using a validation data-set, MLP method has a slightly higher average difference but smaller maximum difference. In real world testing with the SEA hardware, the MLP method shows 27.5% less average force error than the SF method. However, SF method costs 84.6% less average settling time than the MLP method. The surface fitting approach can run on a micro-controller due to its simplicity. The performance comparison of both methods on validation data-set is showed in Tab. V.

Both methods have decent accuracy and acceptable settling time. For applications which do not require low settling time and have ample computational power, the MLP approach is

TABLE IV
FORCE CALIBRATION PERFORMANCE COMPARISON

Method	Error avg	Error max	Error avg	Error max
Kinematics Calc	3.55N	9.38N	34.31%	44.7%
SF(MAE)	0.886N	7.261N	8.06%	35.72%
MLP(MSE)	1.120N	5.304N	10.18%	29.13%

TABLE V
SEA FORCE CONTROL SIMULATION PERFORMANCE COMPARISON

Method	Error avg	Error max	Error avg	Error max
SF(MAE)	0.347mm	1.946mm	7.99%	38.15%
MLP(MSE)	0.409mm	1.505mm	9.38%	30.00%

slightly more accurate. The surface fitting method is suitable for micro-controller applications, where computational power is limited. The surface fitting method is also ideal for application where controlling speed is critical.

X. FUTURE WORK

There are three aspects of this research that can be further improved.

First, a high dimension non-linear fit might have a more accurate result over the linear surface fitting approach. This approach might not be as accurate compared to the MLP approach but might be faster.

Second, the training data-set only had around 10,000 data points, which is considered a relatively small data-set. The size of the data-set might affect the MLP approach. Extending the data-set might further improve the accuracy of both surface fitting and MLP approaches.

Third, this experiment proved that the SEA-based exoskeleton glove needs calibration to achieve a reasonable force measurement result. The error arises when force is transformed from the spring to the fingertips. Unlike most SEA applications used in upper and lower limbs, the SEAs and linkage used in exoskeleton gloves are usually made from plastic or aluminum due to weight and size constraints. The above limitations make these linkages and SEAs easy to deform and affect the accuracy of the force output. These errors are hard to overcome. To solve this issue, Chinpon, *et al.* and Park, *et al.* proposed and verified a possible optical fiber solution to substitute the SEA as an accurate tactile sensor [16], [17]. The optical fiber approach seems to have high accuracy while remaining small in size.

ACKNOWLEDGMENT

The authors would like to thank Isaac Pressgrove and Liu Yujiong who provided valuable advice and greatly assisted in this research.

REFERENCES

- [1] R. Bernstein, "Nearly 1 in 5 people have a disability in the U.S." Census Bur., Suitland-Silver Hill, MD, USA, Tech. Rep. CB12-134, 2012. [Online]. Available: <https://www.census.gov/newsroom/releases/archives/miscellaneous/cb12-134.html>
- [2] J. B. Lee, "Development of intelligent exoskeleton grasping through sensor fusion and slip detection development of intelligent exoskeleton grasping." Ph.D. dissertation, Virginia Polytech. Inst. State Univ., Blacksburg, VA, USA, 2018.

- [3] D. Giovanelli and E. Farella, "Force sensing resistor and evaluation of technology for wearable body pressure sensing," *J. Sensors*, vol. 2016, pp. 1–13, Feb. 2016.
- [4] Z. Ma, P. Ben-Tzvi, and J. Danoff, "Sensing and force-feedback exoskeleton robotic (SAFER) glove mechanism for hand rehabilitation," in *Proc. ASME Int. Des. Eng. Tech. Conf. Comput. Inf. Eng. Conf., 39th Mech. Robot. Conf.*, vol. 5A. Boston, MA, USA: ASME, Aug. 2015, Paper V05AT08A036, doi: [10.1115/DETC2015-46661](https://doi.org/10.1115/DETC2015-46661).
- [5] J. A. Díez, A. Blanco, J. M. Catalán, F. J. Badesa, L. D. Lledó, and N. García-Aracil, "Hand exoskeleton for rehabilitation therapies with integrated optical force sensor," *Adv. Mech. Eng.*, vol. 10, no. 2, pp. 1–11, 2018.
- [6] G. A. Pratt and M. M. Williamson, "Series elastic actuators," in *Proc. IEEE/RSJ Int. Conf. Intell. Robots Syst.*, vol. 1, Aug. 1995, pp. 399–406.
- [7] H.-G. Kim, J.-W. Lee, J. Jang, S. Park, and C. Han, "Design of an exoskeleton with minimized energy consumption based on using elastic and dissipative elements," *Int. J. Control, Autom. Syst.*, vol. 13, no. 2, pp. 463–474, Apr. 2015.
- [8] N. C. Karavas, N. G. Tsagarakis, and D. G. Caldwell, "Design, modeling and control of a series elastic actuator for an assistive knee exoskeleton," in *Proc. 4th IEEE RAS EMBS Int. Conf. Biomed. Robot. Biomechatronics (BioRob)*, Jun. 2012, pp. 1813–1819.
- [9] P. Agarwal, J. Fox, M. K. O'Malley, A. D. Deshpande, and Y. Yun, "An index finger exoskeleton with series elastic actuation for rehabilitation: Design, control and performance characterization," *Int. J. Robot. Res.*, vol. 34, no. 14, pp. 1747–1772, Oct. 2015.
- [10] M. Bianchi *et al.*, "Design of a series elastic transmission for hand exoskeletons," *Mechatronics*, vol. 51, pp. 8–18, May 2018.
- [11] I. Jo and J. Bae, "Design and control of a wearable and force-controllable hand exoskeleton system," *Mechatronics*, vol. 41, pp. 90–101, Feb. 2017, doi: [10.1016/j.mechatronics.2016.12.001](https://doi.org/10.1016/j.mechatronics.2016.12.001).
- [12] E. M. Refour, B. Sebastian, R. J. Chauhan, and P. Ben-Tzvi, "A general purpose robotic hand exoskeleton with series elastic actuation," *J. Mech. Robot.*, vol. 11, no. 6, pp. 1–9, Dec. 2019.
- [13] W. Xu, S. Pradhan, Y. Guo, B.-T. Pinhas, and C. Bravo, "A novel design of a robotic glove system for patients with brachial plexus injuries," in *Proc. ASME IDETC/CIE, 44th Mech. Robot. Conf.*, St. Louis, MO, USA, 2020, Art. no. V010T10A042.
- [14] T. Nilsen, M. Hermann, C. S. Eriksen, H. Dagfinrud, P. Mowinkel, and I. Kjekken, "Grip force and pinch grip in an adult population: Reference values and factors associated with grip force," *Scandin. J. Occupational Therapy*, vol. 19, no. 3, pp. 288–296, May 2012.
- [15] T. Vanteddu, B. Sebastian, and P. Ben-Tzvi, "Design optimization of RML glove for improved grasp performance," in *Proc. ASME Dyn. Syst. Control Conf. (DSCC)*, vol. 1, Sep. 2018, pp. 1–8.
- [16] Y.-L. Park, S. C. Ryu, R. J. Black, K. K. Chau, B. Moslehi, and M. R. Cutkosky, "Exoskeletal force-sensing end-effectors with embedded optical fiber-Bragg-grating sensors," *IEEE Trans. Robot.*, vol. 25, no. 6, pp. 1319–1331, Dec. 2009.
- [17] A. Chinpon, K. Thamaphat, M. Hansuparnusorn, and P. Limsuwan, "A force measurement method using the optical fibre beam," *Procedia Eng.*, vol. 32, pp. 989–993, Jan. 2012, doi: [10.1016/j.proeng.2012.02.043](https://doi.org/10.1016/j.proeng.2012.02.043).



Yunfei Guo received the B.S. and M.S. degrees in electrical and computer engineering from Virginia Tech, VA, USA, in 2019 and 2020, respectively, where he is pursuing the Ph.D. degree in electrical and computer engineering. His research interests are in machine learning applications in embedded systems and ubiquitous computing.



Wenda Xu received the B.S. degree in mechanical engineering from Hunan University, Hunan, China, in 2016, and the M.S. degree in mechanical engineering from Columbia University, NY, USA, in 2019. He is currently pursuing the Ph.D. degree with Virginia Tech, VA, USA. His research interests include robotics design, artificial intelligence, and machine learning.



Sarthark Pradhan received the B.Tech. degree in mechanical engineering from Indian Institute of Technology Bhubaneswar, India, in 2017. He is currently pursuing the master's degree in mechanical engineering with Virginia Tech, VA, USA. His research interests include exoskeletons, humanoid robots, machine learning and motion planning, and localization of robots.



2005. He is certified by the American Board of Orthopaedic Surgery in orthopedics and hand surgery.

Cesar Bravo received the B.S. degree in biomedical engineering, the B.A. degree in applied math and science, and the medical (*magna cum laude*) degree from the University of Puerto Rico School of Medicine. After completing an internship in general surgery and his residency in orthopaedic surgery there, he completed a fellowship in hand surgery at the Mayo Clinic in 2005. He has been specialized in hand and upper extremity surgery with a particular interest in problems of the elbow with Carilion Clinic since



2005. He is certified by the American Board of Orthopaedic Surgery in orthopedics and hand surgery.

Pinhas Ben-Tzvi (Senior Member, IEEE) received the B.S. (*summa cum laude*) degree in mechanical engineering from the Technion-Israel Institute of Technology, Haifa, Israel, and the M.S. and Ph.D. degrees in mechanical engineering from the University of Toronto, Toronto, Canada. He is currently a Professor of Mechanical Engineering and Electrical and Computer Engineering, and the Founding Director of the Robotics and Mechatronics Laboratory, Virginia Tech. His current research interests include robotics and intelligent autonomous systems, human-robot interactions, robotic vision and visual servoing, machine learning, mechatronics design, systems dynamics and control, mechanism design and system integration, and novel sensing and actuation. His research program has been supported by NSF, NIH, DARPA, ONR, USN, USAMRMC/TATRC, and NAVO. He has authored or coauthored more than 165 peer-reviewed journal articles and refereed papers in conference proceedings and the named inventor on at least 12 U.S. patents and patent applications. He is a member of ASME. He was a recipient of the 2019 Virginia Tech Excellence in Teaching Award, the 2018 Virginia Tech Faculty Fellow Award, the 2013 GWU SEAS Outstanding Young Researcher and Outstanding Young Teacher Awards, and several other honors and awards. He served as an Associate Editor for IEEE ICRA from 2013 to 2018. He is also a Technical Editor of the IEEE/ASME TRANSACTIONS ON MECHATRONICS, and an Associate Editor of ASME *Journal of Mechanisms and Robotics* and IEEE *Robotics and Automation Magazine*.